# Macroscopic direct observation of optical spin-dependent lateral forces and left-handed torques

Hernando Magallanes, Etienne Brasselet

# Macroscopic direct observation of optical spin-dependent lateral forces and left-handed torques

Hernando Magallanes and Etienne Brasselet*

**Observing and taming the effects arising from non-trivial light–matter interaction has always triggered scientists to better understand nature and develop photonic technologies. However, despite tremendous conceptual advances[1,2], so far there have been only a few experimental proposals to reveal unusual optomechanical manifestations that are hardly seen in everyday life, such as negative radiation pressure[3,4], transverse forces[5,6] or left-handed torques[7]. Here, we report naked-eye identification of spin-dependent lateral displacements of centimetre-sized objects endowed with structured birefringence. Left-handed macroscopic rotational motion is also reported. The unveiled effects ultimately rely on spin–orbit optical interactions and are driven by lateral force fields that are five orders of magnitude larger than those reported previously, as a result of the proposed design. By highlighting the spin–orbit optomechanics of anisotropic and inhomogeneous media, these results allow structured light–matter interaction to move from a scientific curiosity to a new asset for the optical manipulation toolbox.**

In free space, paraxial light carries longitudinal linear and angular momenta, both pointing along the propagation direction, as their names suggest. The collinearity between the incident momenta and the direction of the radiation forces ($\mathbf{F}$) and torques ($\boldsymbol{\Gamma}$) exerted by light on matter is, however, not a rule of thumb. For example, for a beam reflecting off a perfect mirror, it is well understood that both $\mathbf{F}$ and $\boldsymbol{\Gamma}$ lie in the incidence plane. The situation becomes more complex when an object is placed near an interface, even in the simplest case of a planar surface separating two semi-infinite media, where optical forces and torques transverse with respect to the driving flow of light can appear. This was discussed theoretically for particles placed in the evanescent field of dielectric[8] or plasmonic[9] interfaces, and was soon followed by the first experimental demonstrations of spin-dependent lateral forces[5,6]. Besides the case of pure surface waves, the back-action of guided modes in the presence of material spatial confinement has also been explored for circularly oscillating light-induced[10] or spontaneously emitting[11] dipoles. Other schemes have been proposed, for instance by placing a spinning particle in the path of a light beam[12] or by using inhomogeneous light fields[13–15]. Finally, we also mention early theoretical efforts to deploy spin-dependent lateral forces to sort material chirality by chiral light[16–20].

Surprisingly, only a few spin–orbit optical experiments report on the direct observation of spin-dependent lateral forces[5,6,21], and these are all based on micrometre-sized objects and involve force magnitudes of up to 1–10 fN, associated with a lateral displacement of up to 0.1–10 μm. Furthermore, these are associated with instrumental[5,6] or interpretation[21] difficulties. For example, force enhancement via many-particle hydrodynamic interactions is needed in ref. [5], and polarization-resolved reconstruction of both the longitudinal and transverse force components, based on symmetry considerations, is required in ref. [6]. In contrast, here we report observation of these forces using centimetre-sized objects experiencing lateral forces on the order of 1 nN that lead to displacements over a distance of up to 0.5 mm in less than 100 s, with an incident optical power of 1 W. Our macroscopic experiment thus deals with an increase in the force per unit power by five orders of magnitude compared to previous works.

In practice, 'spin up' (↑) and 'spin down' (↓) photons are selectively steered on either side of the direction of propagation of the incident light by using one-dimensional space-variant geometric phase elements[22] made of a transparent anisotropic (uniaxial) medium with uniform birefringent phase retardation $\Delta$ and optical axis orientation angle $\psi(x) = \pm 2\pi x/\Lambda$, where $\Lambda$ is the distance over which the optical axis makes a full turn and $(x, y)$ defines the plane of the sample (Fig. 1). These optical elements are characterized by suppression of all diffraction orders except the $\pm$1st ones, provided that $\Delta = \pi$ (ref. [23]). Here, the system is made of a structured liquid-crystal polymer layer[24] whose thickness and birefringence are designed to fulfil the half-wave birefringent retardation condition at $\lambda = 532$ nm, with $\Lambda \simeq 4.6$ μm, which gives a deflection angle of $\alpha = \arcsin(2\lambda/\Lambda) \simeq 13°$ in air, and spin-flipped transmission. The structural characterization of the material is shown in Fig. 1a, and its spin-dependent diffraction behaviour is reported in Fig. 1b–d for incident spin up and down states, and an even-weight mixture of them. Ensuing direct observation of spin-dependent lateral forces $\mathbf{F}_\perp^{(\uparrow,\downarrow)}$, which satisfy $\mathbf{F}_\perp^{(\uparrow)} \cdot \mathbf{F}_\perp^{(\downarrow)} < 0$ and $|\mathbf{F}_\perp^{(\uparrow)}| = |\mathbf{F}_\perp^{(\downarrow)}|$, thus depends on the ability to design an experiment where the light-induced motion of the sample is not hindered.

As shown in Fig. 2a, the sample was placed at an air–water interface in a 7 cm × 1 cm rectangular Plexiglass pool with 5 mm depth, taking care to fix the solid–liquid–gas contact line at the rim of the slightly under-filled pool. The two main menisci, with different radii of curvature, thus ensure capillary alignment and stable trapping of a 6 mm × 1 mm rectangular sample in the centre of the pool, as long as the laser beam is off (Fig. 2b). Qualitative optomechanical observations are shown in Fig. 2c when in the presence of a laser beam with incident power $P$ of ~1 W for left-handed circular, linear and right-handed circular incident polarization states, respectively (Supplementary Video 1). The sample does not move in the case of linear polarization, but it moves and eventually stops as it gets closer to the meniscus for circular polarizations. Indeed, the meniscus behaves as a capillary spring loading with sample displacement. Moreover, opposite lateral displacements with the same order of magnitude are observed when photons are prepared in either up or down spin states.

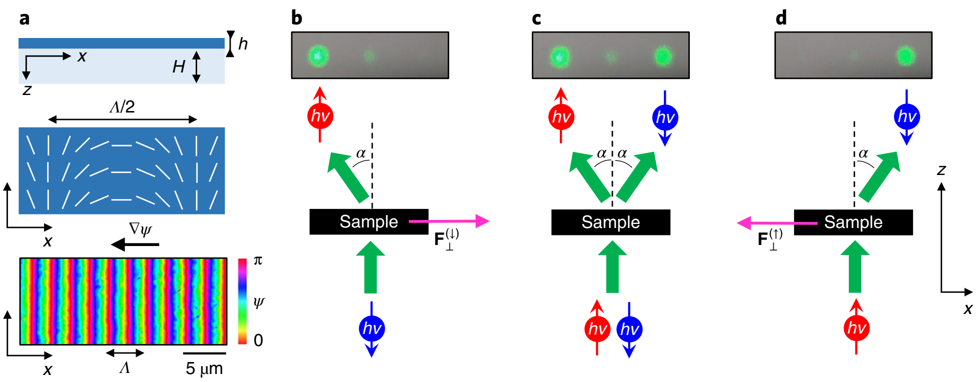


**Fig. 1 | Spin-dependent lateral optical forces from spin-orbit scattering by a one-dimensional geometric phase optical element. a**, The material consists of a one-dimensional geometric phase optical element of thickness $h$ (~2 μm) that is deposited on a transparent flexible plastic sheet of thickness $H$ (~200 μm). Optical microscopy birefringent imaging reveals the one-dimensional periodic modulation of the optical axis orientation angle in the plane of the sample, here $\psi = -2\pi x/\Lambda$. **b**–**d**, Spin-dependent beam steering associated with the deflection angle $\alpha$ (ref. [22]) of the transmitted photons leads to spin-dependent lateral optical forces $F_\perp^{(\uparrow,\downarrow)}$ with opposite direction and the same magnitude for incident spin up and down (**b**,**d**) and no net lateral force for incident linearly polarized light carrying equal-weight fractions of spin up and down photons (**c**). Corresponding experimental diffraction patterns are shown on the upper parts of **b**–**d**.

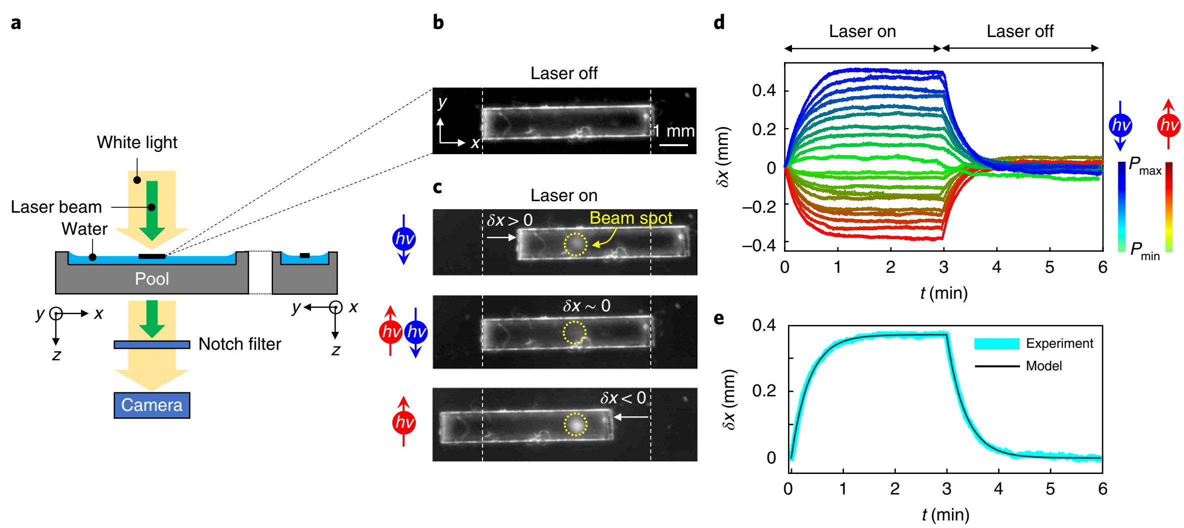


**Fig. 2 | Macroscopic direct observation of spin-dependent lateral optical forces. a**, The sample is a 6 mm × 1 mm handcut rectangular slab placed at the air-water interface of a 7 cm × 1 cm rectangular Plexiglass pool with 5 mm depth. **b**, At rest, the sample is self-aligned and trapped in the centre of the pool by capillary effects. The optomechanical effect is driven by a normally incident Gaussian laser beam with 0.9 mm waist diameter centred on the sample at rest. The sample dynamics were video-recorded by a camera under unpolarized white light illumination with almost total extinction of the spin–orbit-scattered laser light by placing a spectrally selective so-called Notch filter (532 nm wavelength) in front of the camera. **c**, Typical steady-state spin-dependent displacement under ~1 W incident optical power. **d**, Power and spin dependence of excitation/relaxation dynamics for ten values of incident power between $P = 0.14$ W and $P = 1.4$ W in 0.14 W steps, for both spin up and spin down cases. Each curve is the average of three independent events. **e**, Typical quantitative description of translational dynamics using a linear damped oscillator model (see main text).

Quantitative analysis was carried out by recording the excitation and relaxation dynamics of the sample, $x(t)$, as summarized in Fig. 2d for ten values of incident power for both spin up and down cases. Each curve is the average of three on–off cycles for the laser irradiation, each cycle consisting of 3 min irradiation followed by 3 min relaxation, which allowed reliable data analysis. A simple yet relevant model of a linear forced oscillator with damping model is proposed, $m\ddot{x} + \gamma\dot{x} + \kappa x = H(t)F_\perp$, where $m = 1.6$ mg is the mass of the sample, $\gamma$ refers to the losses arising mainly from the viscosity of water, $\kappa$ is the effective spring constant associated with the curved air–water interface, $H$ is a step function defined as $H(0 < t < t_{\rm off}) = 1$ and $H(t > t_{\rm off}) = 0$, with time zero taken as the moment when the laser is switched on from the situation at rest, and $(\dot{x}, \ddot{x})$ stands for $(dx/dt, d^2x/dt^2)$. According to the boundary conditions for the excitation and relaxation regimes (which assumes large enough $t_{\rm off}$ with respect to the transient excitation time), $\{x(0) = 0, \dot{x}(0) = 0\}$ and $\{x(t_{\rm off}) = F_\perp/\kappa, \dot{x}(t_{\rm off}) = 0\}$, the equations of motion are

$$x_{\rm on}(0 < t < t_{\rm off}) = \frac{F_\perp}{\kappa}\left[1 + \frac{\beta_- e^{\beta_+ t} - \beta_+ e^{\beta_- t}}{\beta_+ - \beta_-}\right]$$

and

$$x_{\rm off}\ (t > t_{\rm off}) = \frac{F_\perp}{\kappa}\frac{\beta_- e^{\beta_+ (t - t_{\rm off})} - \beta_+ e^{\beta_- (t - t_{\rm off})}}{\beta_- - \beta_+},$$

with $\beta_\pm = \left(-\gamma \pm \sqrt{\gamma^2 - 4m\kappa}\right) / (2m)$ and where we use the Minkowski expression for the spin-dependent lateral force, $F_\perp = \pm(P/c)\sin\theta$. A typical fit of the experimental data is shown in Fig. 2e, with $\{\gamma, \kappa\}$ being two adjustable parameters that are typically $\gamma \sim 40\,{\rm mg\,s^{-1}}$ and $\kappa \sim 2\,{\rm mg\,s^{-2}}$.

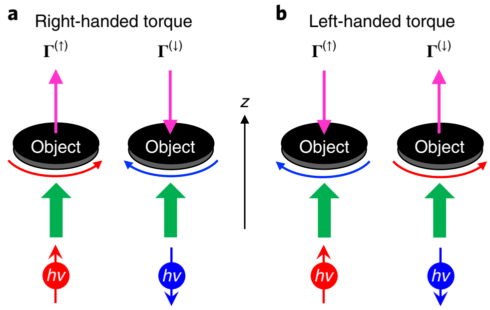


**Fig. 3 | Principle of right- and left-handed optical radiation torques.** **a**, An object subjected to the application of a usual optical torque ('right-handed') controlled by the spin angular momentum of light tends to rotate in the same direction as the incident angular momentum. **b**, The reverse situation corresponds to unconventional ('left-handed') optical torque manifestation.

Towards the generalization of the above results, we recall that a torque is associated with a spatial distribution of transverse elementary forces. Therefore, because $\mathbf{F}_\perp \times \nabla\psi = 0$, arbitrary spin-driven optical torques can be formally designed from appropriate material structuring. In particular, we address the direct observation of an unusual effect earlier referred to the existence of a 'left-handed' optical torque[7] where the applied total torque $\boldsymbol{\Gamma}$ and incident spin optical angular momentum $\mathbf{S}$ are anti-parallel, $\boldsymbol{\Gamma}\cdot\mathbf{S} < 0$, in contrast to a 'right-handed' torque where $\boldsymbol{\Gamma}\cdot\mathbf{S} > 0$, as illustrated in Fig. 3. An early numerical prediction of left-handed torques was reported in ref. [25], using wavelength-sized prolate particles made of transparent isotropic medium under tightly focused circularly polarized Gaussian beams. Since then, several alternative routes have been discussed theoretically[26–29]. However, so far there has been no direct experimental observation of such an effect.

Here we propose to reverse the indirect approach reported in ref. [7], where the mechanical action of matter on light was analysed, by directly looking at the mechanical action of light on matter. We fabricated ~6-mm-diameter four-quadrant disk-shaped spin–orbit rotors according to the design shown in Fig. 4a. The orientational gradients $\nabla\psi$ are oriented anticlockwise (right-handed case) or clockwise (left-handed case), respectively. In practice, the four pieces are deposited at the air–water interface of a 2-cm-diameter slightly under-filled 5-mm-deep circular Plexiglass pool where they remain bound via capillary effects. Recalling that $\boldsymbol{\Gamma} = \iint \mathbf{r}\times\mathbf{F}_\perp \mathrm{d}x\mathrm{d}y$ and $|\mathbf{F}_\perp| \propto I$, where $I$ refers to the spatial distribution of the light intensity, the torque magnitude is optimized by shaping the incident beam in a ring fashion using an axicon placed before a lens. The obtained axisymmetric intensity profile is described by three parameters ($\eta_0$, $r_0$ and $w_0$) according to the analytical expressions $I(r)/I_{\max} = \eta_0 + (1-\eta_0)e^{-2(r-r_0)^2/w_0^2}$ for $r < r_0$, and $I(r)/I_{\max} = e^{-2(r-r_0)^2/w_0^2}$ for $r > r_0$ (Fig. 4b). This model allows us to evaluate that our experimental conditions correspond to a torque magnitude $|\Gamma| = \frac{4\sin\alpha}{c}\int_0^R I(r)r^2\mathrm{d}r$ that is ~75% of the expected ideal value (Fig. 4c).

Qualitative observations for spin up and down incident photons for both right-handed and left-handed situations at fixed incident power are displayed in Fig. 4d that shows a light-induced angular deviation $\theta$ (Supplementary Video 2). Typical excitation/relaxation rotational dynamics are presented in Fig. 5a, which shows the average of three independent events. As for the lateral displacement experiments, the dynamics are quantitatively described by a linear damped oscillator model that is readily obtained according to the changes $x \leftrightarrow \theta$ and $m \leftrightarrow \frac{1}{2}mR^2$. The losses still arising (mainly from the viscosity of water) are taken into account by coefficient $\gamma$, while $\kappa$ relates to a torsional spring probably arising from elasticity associated with the out-of-plane contact line around the uneven handcut sample, which prevents light-induced spinning. The power dependence of the effect is shown in Fig. 5b, where the right- and left-handed nature of the driving optical torque is inferred by looking at the sign of the product $\sigma\theta_\infty$, where $\sigma = \pm 1$ is the incident helicity ($\sigma = +1$ for spin up and $\sigma = -1$ for spin down) and $\theta_\infty$ is the steady angular deviation under constant irradiation power. Indeed, $\boldsymbol{\Gamma}\cdot\mathbf{S}$ and $\sigma\theta_\infty$ have the same sign. In addition, we emphasize the large value of the optical torque per unit power estimated from $|\Gamma|/P = \frac{2\sin\alpha}{\pi c}\int_0^R I(r)r^2\mathrm{d}r / \int_0^\infty I(r)r\mathrm{d}r$, which is of the order of 1 pNm W$^{-1}$ for our samples (Fig. 5c). Finally, it is instructive to mention that the present macroscopic samples behave as effective so-called $q$-plates[30] with structural topological charges $|q_{\mathrm{eff}}| \sim 1{,}700$ (Fig. 5d). This is deduced by balancing the above torque expression

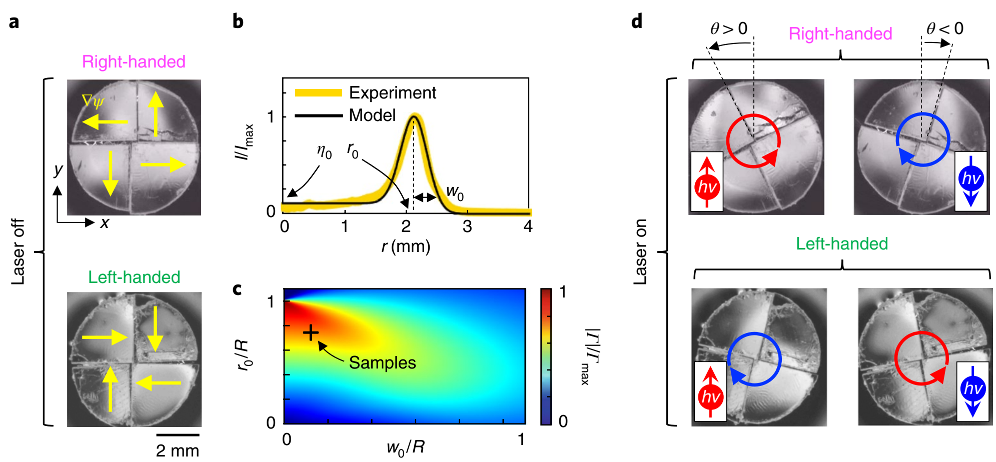


**Fig. 4 | Macroscopic direct observation of the angular analogue of lateral optical forces.** **a**, Disk-shaped capillary-bound handcut four-quadrant spin-orbit rotors (radius $R \sim 3$ mm) placed at the air-water interface of a 2-cm-diameter circular Plexiglass pool (5 mm deep). Two samples with opposite spatial distribution of the orientational gradients $\nabla\psi$ are prepared to ensure either right-handed or left-handed effects. **b**, Azimuth-averaged ring-shaped experimental radial intensity profile in the plane of the sample and its adjustment using the ansatz function given in the text, which gives values of $\eta_0 = 0.12$, $r_0 = 0.73R$ and $w_0 = 0.15R$ for the three adjustable parameters. Corresponding experimental and calculated transverse intensity profiles are shown. **c**, Calculated normalized optical torque magnitude on an ideal four-quadrant disk irradiated by circularly polarized incident light as a function of the reduced parameters $r_0/R$ and $w_0/R$ at fixed power and imposing $\eta_0 = 0.12$, where $\Gamma_{\max}$ refers to the maximum of $|\Gamma|$. The cross marker indicates the sample characteristics. **d**, Typical steady-state angular deviation $\theta$ (of the sample in the $(x,y)$ plane) associated with right-handed and left-handed optical torque experiments for incident spin up and spin down photons, for a total incident optical power $P$ of ~3 W.

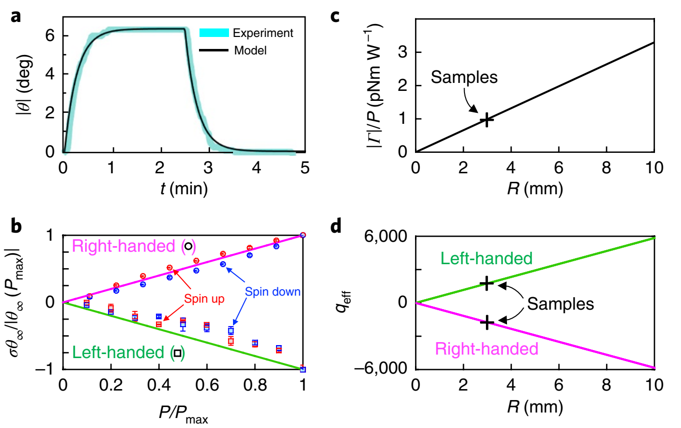


**Fig. 5 | Quantitative analysis of right- and left-handed optical radiation torque. a**, Typical quantitative description of excitation/relaxation rotational dynamics using a linear damped oscillator model, which in our experiments typically gives $\gamma \sim 60$ mg mm$^2$ s$^{-1}$ and $\kappa \sim 10$ mg mm$^2$ s$^{-2}$. **b**, Power dependence of $\sigma\theta_\infty/|\theta_\infty(P_{\max})|$, with $P_{\max} \sim 3$ W, the sign of which allows straightforward identification of the right-handed and left-handed nature of the applied optical torque. Error bars show standard deviation of three independent dynamic events. **c**, Calculated torque per unit power as a function of radius of an ideal four-quadrant disk irradiated by a circularly polarized incident ring-shaped beam in the sample plane, using the actual beam parameters. **d**, Estimated structural topological charge $q_{\rm eff}$ of an equivalent effective $q$-plate with radius $R$ (see main text for details).

with that of the spin–orbit torque exerted on a $q$-plate irradiated by a circularly polarized beam of power $P$, $2\sigma(1-q_{\rm eff})P/\omega$ (ref. [7]), which gives $q_{\rm eff} = 1 \mp |\Gamma|\omega/2P$ for the right- and left-handed cases, respectively.

These results show that direct experimental observations of unusual optomechanical manifestations are restricted neither to tricky instrumental approaches nor to weak transverse effects vanishing in the single-dipole limit. This indicates that structured anisotropic matter is a wonderful playground for exploring new facets of light–matter interactions, which do not necessarily require the use of coherent light sources. So far, geometric phases and spin–orbit interactions have been able to shift light beams[1], but now these are demonstrated to be able to shift matter along independent translational and rotational mechanical degrees of freedom. We therefore anticipate the development of light-driven micromachines made from designer metasurfaces (possibly reconfigurable), for example, for micro-rheological applications such as linear and rotational shearing of soft matter at a small scale.

**Data availability.** The data that support the findings of this study are available from the corresponding author upon reasonable request.

## References

1. Bliokh, K. Y., Rodrguez-Fortuño, F. J., Nori, F. & Zayats, A. V. Spin–orb t interactions of light. *Nat. Photon.* **9**, 796–808 (2015).
2. Sukhov, S. & Dogariu, A. Non-conservative optical forces. *Rep. Prog. Phys.* **80**, 112001 (2017).
3. Brzobohaty, O. et al. Experimental demonstration of optical transport, sorting and self-arrangement using a 'tractor beam'. *Nat. Photon.* **7**, 123–127 (2013).
4. Dogariu, A., Sukhov, S. & Saenz, J. J. Optically induced 'negative forces'. *Nat. Photon.* **7**, 24–27 (2013).
5. Sukhov, S., Kajorndejnukul, V., Naraghi, R. R. & Dogariu, A. Dynamic consequences of optical spin–orbit interaction. *Nat. Photon.* **9**, 809–812 (2015).
6. Antognozzi, M. et al. Direct measurements of the extraordinary optical momentum and transverse spin-dependent force using a nano-cantilever. *Nat. Phys.* **12**, 731–735 (2016).
7. Hakobyan, D. & Brasselet, E. Left-handed optical radiation torque. *Nat. Photon.* **8**, 610–614 (2014).
8. Bliokh, K. Y., Bekshaev, A. Y. & Nori, F. Extraordinary momentum and spin in evanescent waves. *Nat. Commun.* **5**, 3300 (2014).
9. Canaguier-Durand, A. & Genet, C. Transverse spinning of a sphere in a plasmonic field. *Phys. Rev. A* **89**, 033841 (2014).
10. Rodrguez-Fortuño, F. J., Engheta, N., Martnez, A. & Zayats, A. V. Lateral forces on circularly polarizable particles near a surface. *Nat. Commun.* **6**, 8799 (2015).
11. Scheel, S., Buhmann, S. Y., Clausen, C. & Schneeweiss, P. Directional spontaneous emission and lateral Casimir–Polder force on an atom close to a nanofiber. *Phys. Rev. A* **92**, 043819 (2015).
12. Movassagh, R. & Johnson, S. G. Optical Bernoulli forces. *Phys. Rev. A* **88**, 023829 (2013).
13. Sukhov, S., Kajorndejnukul, V., Broky, J. & Dogariu, A. Forces in Aharonov–Bohm optical setting. *Optica* **1**, 383–387 (2014).
14. Bekshaev, A. Y., Bliokh, K. Y. & Nori, F. Transverse spin and momentum in two-wave interference. *Phys. Rev. X* **5**, 011039 (2015).
15. Fardad, S. et al. Scattering detection of a solenoidal Poynting vector field. *Opt. Lett.* **41**, 3615–3618 (2016).
16. Wang, S. B. & Chan, C. T. Lateral optical force on chiral particles near a surface. *Nat. Commun.* **5**, 3307 (2014).
17. Cameron, R. P., Barnett, S. M. & Yao, A. M. Discriminatory optical force for chiral molecules. *New J. Phys.* **16**, 013020 (2014).
18. Hayat, A., Mueller, J. B. & Capasso, F. Lateral chiral ty-sorting optical forces. *Proc. Natl Acad. Sci. USA* **112**, 13190–13194 (2015).
19. Canaguier-Durand, A. & Genet, C. Plasmonic lateral forces on chiral spheres. *J. Opt.* **18**, 015007 (2015).
20. Alizadeh, M. & Reinhard, B. M. Transverse chiral optical forces by chiral surface plasmon polaritons. *ACS Photon.* **2**, 1780–1788 (2015).
21. Cipparrone, G., Hernandez, R. J., Pagliusi, P. & Provenzano, C. Magnus force effect in optical manipulation. *Phys. Rev. A* **84**, 015802 (2011).
22. Bomzon, Z., Biener, G., Kleiner, V. & Hasman, E. Space-variant Pancharatnam–Berry phase optical elements with computer-generated subwavelength gratings. *Opt. Lett.* **27**, 1141–1143 (2002).
23. Nikolova, L. & Todorov, T. Diffraction efficiency and selectivity of polarization holographic recording. *Opt. Acta* **31**, 579–588 (1984).
24. Tabiryan, N. V., Nersisyan, S. R., Steeves, D. M. & Kimball, B. R. The promise of diffractive waveplates. *Opt. Photon. News* **21**, 41–45 (2010).
25. Simpson, S. H. & Hanna, S. Optical trapping of spheroidal particles in Gaussian beams. *J. Opt. Soc. Am. A* **24**, 430–443 (2007).
26. Haefner, D., Sukhov, S. & Dogariu, A. Conservative and nonconservative torques in optical binding. *Phys. Rev. Lett.* **103**, 173602 (2009).
27. Chen, J. et al. Negative optical torque. *Sci. Rep.* **42**, 6386 (2014).
28. Nieto-Vesperinas, M. Optical torque on small bi-isotropic particles. *Opt. Lett.* **40**, 3021–3024 (2015).
29. Canaguier-Durand, A. & Genet, C. Chiral route to pulling optical forces and left-handed optical torques. *Phys. Rev. A* **92**, 043823 (2015).
30. Marrucci, L., Manzo, C. & Paparo, D. Optical spin-to-orbital angular momentum conversion in inhomogeneous anisotropic media. *Phys. Rev. Lett.* **96**, 163905 (2006).

## Acknowledgements

This study received financial support from CONACYT Mexico.

## Author contributions

H.M. realized the experimental set-up, conducted the experiments and analysed data. E.B. conceived the experiment, analysed data and supervised the project. E.B. wrote the paper.

## Competing interests

The authors declare no competing interests.

**Correspondence and requests for materials** should be addressed to E.B.